Applied Energy 108 (2013) 340–348

Contents lists available at SciVerse ScienceDirect

Applied Energy

journal homepage: www.elsevier.com/locate/apenergy

Transient modeling and dynamic characteristics of thermoelectric cooler

Jing-Hui Meng [a], Xiao-Dong Wang [b,c,*], Xin-Xin Zhang [a]

[a] School of Mechanical Engineering, University of Science and Technology Beijing, Beijing 100083, China
[b] State Key Laboratory of Alternate Electrical Power System with Renewable Energy Sources, North China Electric Power University, Beijing 102206, China
[c] Beijing Key Laboratory of Multiphase Flow and Heat Transfer for Low Grade Energy, North China Electric Power University, Beijing 102206, China

HIGHLIGHTS

- A complete three-dimensional TEC transient model was proposed.
- The model couples heat conduction and electric conduction.
- Dynamic behaviors are studied at extensive operating conditions.
- Temperature-dependent material properties have strong effect on dynamic behaviors.

ARTICLE INFO

Article history:
Received 18 October 2012
Received in revised form 10 January 2013
Accepted 22 March 2013
Available online 11 April 2013

Keywords:
Thermoelectric cooler
Dynamic characteristics
Heat transfer
Peltier
Seebeck
Thomson

ABSTRACT

Dynamic characteristics are extremely important for design and operation of thermoelectric coolers (TECs). This paper develops a three-dimensional transient TEC model based on the coupling of heat transfer and electric conduction within semiconductors. The model takes into account all thermoelectric effects, including Joule heating, Thomson effect, Peltier effect and Fourier's heat conduction. For most of semiconductor materials, Seebeck coefficient, electric conductivity and thermal conductivity are strongly temperature-dependent. Therefore, the present transient model is used to compare dynamic temperature variations at the cold and hot ends with constant and variable material properties. Small, medium, and large applied currents with various cooling loads are adopted as operating conditions. The results show that, at small currents, constant property model developed by this work can predict accurately the dynamic characteristics, however, with the increase in current, the temperature-dependence of properties have more and more remarkable effect on the dynamic temperature variations, especially for high cooling loads. When the current is larger than a specific value, the heat transferred from the hot end to the cold end by Fourier's heat conduction will exceed the heat adsorbed at the cold end by Peltier effect, thus, the temperatures at the cold and hot ends increase continuously, the TEC cannot reach the steady-state. This phenomena is predicted exactly by the variable property model, oppositely, the constant property model predicts that the TEC still supply refrigeration.

1. Introduction

In recent years, TECs have attracted more and more attention due to their features of no compressors and refrigerants, large operating temperature range, easy to control, reliable operation, layout flexibility, adaptability and other characteristics [1–3]. The TEC has been frequently used for the cooling of electric devices such as CPU, infrared sensor, ice-point reference in thermocouple thermometry, and refrigerators [4]. Generally, the TEC includes a number of thermoelectric elements, which are connected electrically in series and thermally in parallel. The thermoelectric elements are composed of a pair of p- and n-type semiconductors. When electric current flows across the thermoelectric elements, the heat is transported from the cold end to the hot end caused by the Peltier effect.

A large amount of works considered the TEC performance [5–13] and the TEG performance [14–22] under steady-state condition, while few works [4,23–29] investigated its transient or dynamic characteristics. Actually, transient characteristics are also extremely important in practical TEC operation. First, cooling load at the cold end and/or cooling capacity of heat sink and ambient temperature at the hot end may be variable [24]. Second, the start up and shut down characteristics of TECs are also a major concern for cooling purpose [25,26]. For example, for a fixed cooling load at the cold end and a fixed cooling capacity of heat sink at the hot end, when a specific current is applied to the TEC, how much is the consuming for the TEC to reach the steady-state and what

* Corresponding author at: State Key Laboratory of Alternate Electrical Power System with Renewable Energy Sources, North China Electric Power University, Beijing 102206, China. Tel./fax: +86 10 62321277.
E-mail address: wangxd99@gmail.com (X.-D. Wang).

0306-2619/$ - see front matter © 2013 Elsevier Ltd. All rights reserved.
http://dx.doi.org/10.1016/j.apenergy.2013.03.051

are the corresponding steady-state temperatures of cold and hot ends. In addition, as a current pulse with a magnitude of several times higher than the steady-state optimum current is applied to a TEC, the transient lower temperature than that reachable at the steady-state can be achieved at the cold end due to the delay of the thermal diffusion of the volumetric Joule heat, which is referred to as the transient thermoelectric effect [27,28].

Up to now, some transient models have been developed to understand the dynamic behaviors of TEC. Mostly the previous transient models were limited to one-dimensional problems [4,24,28], where the Thomson effect was ignored and constant material properties were used because small temperature difference between the cold and hot ends was assumed. In addition, as mentioned by Cheng et al. [26], in the existing models, the p-n element pair was simply treated as a single bulk material so that the difference in thermal behavior between the two semiconductor elements was not possible to evaluate. Hence, Cheng et al. developed a three-dimensional model with p-type and n-type semiconductors as two separate parts and the Thomson effect was taken into account. However, the material properties were still assumed to be constants in the Cheng's model.

Recently, we proposed a general, three-dimensional TEC steady-state model [29], which is different from previous models [5–13] in which only heat conduction equation with Joule heat and/or Thomson heat as internal heat sources is solved. Our model introduced the coupling of heat conduction and electrical conduction, and considered all the effects occurred in the TEC. The model was used to figure out the performance of TECs with the temperature-dependent material properties. The predictions showed that the variable properties and the heat losses to the ambient gas have significant effects on the cooling capacity and the coefficient of performance (COP) of the TEC. Three-dimensional temperature distributions within semiconductors was observed and it became more remarkable at large temperature differences and high currents.

The purpose of this work reaches the following targets: (1) extending our previous steady-state model [29] to a transient one; (2) employing the developed transient model to investigate the dynamic characteristics of TECs under various operating conditions. The dynamic behaviors for TECs with temperature-dependent properties are analyzed and compared with those constant properties.

2. Model development

The schematic of a TEC device containing one semiconductor element pair (referred to as TEC element hereafter) is shown in Fig. 1. A TEC device consists of a number of TEC elements. In consideration that the thermal characteristics among the TEC elements are periodic, hence, only one element is considered here. The TEC element includes a pair of p- and n-type semiconductor columns, three metallic connectors, and two electrically insulating ceramic plates. The ceramic plate, connector, and semiconductor columns have thicknesses of H_0, H_1, and H_2, respectively. The semiconductor columns have square cross-section with the side length of L_2. The distance between p- and n-type semiconductors is L_1. A heat sink with the thickness of H_s is attached on the hot end of the TEC element for heat dissipation. The geometric parameters of the TEC element simulated in the present work are as follows, L_1 = 0.2 mm, L_2 = 0.5 mm, H_0 = 0.2 mm, H_1 = 0.1 mm, H_2 = 1.0 mm, and H_s = 0.2 mm.

When applied current flows from the p-type semiconductor to n-type semiconductor, the holes in the p-type semiconductor and the electrons in the n-type semiconductor migrate from the cold end to the hot end, the corresponding Peltier heats will be generated at the interface between connectors and semiconductors. The heat is adsorbed at the cold end and liberated at the hot end caused by the Peltier effect, forming a temperature difference $\Delta T = T_H - T_L$. With the temperature difference, the heat will be transferred from the hot end to the cold end due to Fourier's heat conduction. In the role of the current and temperature gradient, the Joule heat and the Thomson heat will be generated within semiconductors. Thus the final cooling capacity of the TEC, Q_L, is determined by cooperative effect of Peltier heat, Fourier's heat conduction, Joule heat, and Thomson heat.

2.1. Governing equations

The transient TEC model is developed from our previous steady-state model [29] by adding a transient term. The basic governing equations include the energy equations and the electric potential equations. The energy equations of connectors, p- and n-type semiconductors, ceramic plates, and heat sink are as follows:

$$(\rho c_p)_{\text{conn}} \frac{\partial T}{\partial \tau} = \nabla \cdot (\lambda_{\text{conn}} \nabla T) + \frac{J^2}{\sigma_{\text{conn}}} - \beta_{\text{conn}} \vec{J} \cdot \nabla T \tag{1}$$

$$(\rho c_p)_p \frac{\partial T}{\partial \tau} = \nabla \cdot (\lambda_p \nabla T) + \frac{J^2}{\sigma_p} - \beta_p \vec{J} \cdot \nabla T \tag{2}$$

$$(\rho c_p)_n \frac{\partial T}{\partial \tau} = \nabla \cdot (\lambda_n \nabla T) + \frac{J^2}{\sigma_n} - \beta_n \vec{J} \cdot \nabla T \tag{3}$$

$$(\rho c_p)_{\text{cer}} \frac{\partial T}{\partial \tau} = \nabla \cdot (\lambda_{\text{cer}} \nabla T) \tag{4}$$

$$(\rho c_p)_{\text{sink}} \frac{\partial T}{\partial \tau} = \nabla \cdot (\lambda_{\text{sink}} \nabla T) \tag{5}$$

where ρ is the density, c_p is the specific heat, λ is the thermal conductivity, σ is the electric conductivity, and β is the Thomson coefficient. The subscripts conn, p, n, cer, and sink denote connector, p- and n-type semiconductors, ceramic plate, and heat sink, respectively. The first terms on the right side in Eqs. (1)–(5) denote Fourier's heat conduction, the second and third terms denote internal heat sources due to Joule heating and Thomson effect, respectively. $J(x, y, z)$ is the local current density, which is assumed to be constant and equal to I/A in the previous models [4–13,23–28], where I is the total applied current, and A is the cross-sectional area of semiconductors. The Thomson coefficient can be derived from Seebeck coefficient, or:

$$\beta = T \frac{\mathrm{d}\alpha}{\mathrm{d}T} \tag{6}$$

where α is the Seebeck coefficient. The electric potential is the driving force of the electrons and holes in the semiconductor, which can be obtained by solving the following equation:

$$\nabla \cdot (\sigma(\nabla \phi - \alpha \nabla T)) = 0 \tag{7}$$

where ϕ is the electric potential, $\alpha \nabla T$ is Seebeck electromotive force coming from Seebeck effect. Once ϕ is determined, the electric field can be calculated by the following equation:

$$\vec{E} = -\nabla \phi + \alpha \nabla T \tag{8}$$

Finally, the current density vector in Eqs. (1)–(3) can be calculated as follows:

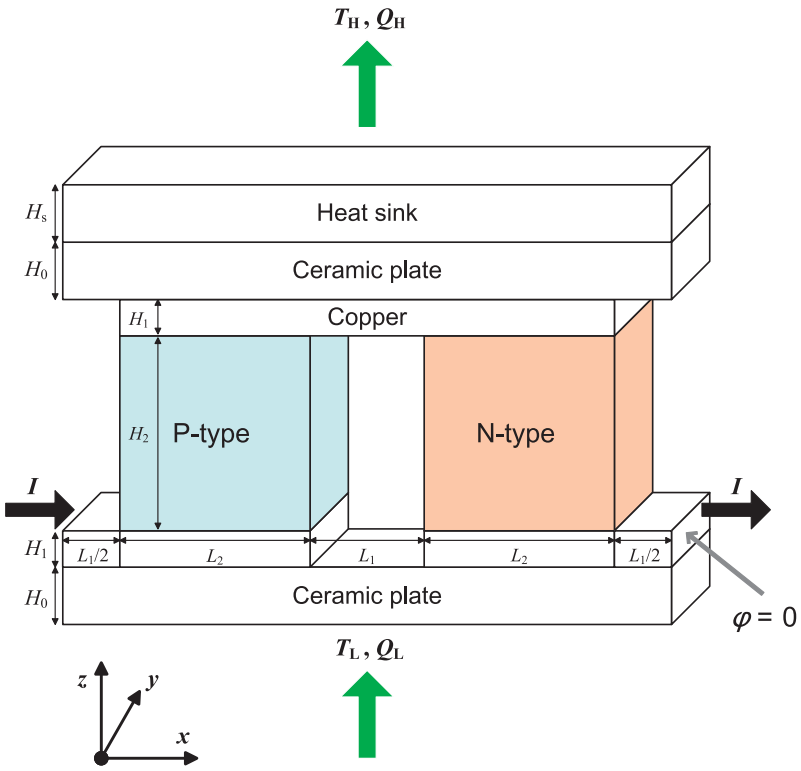

Fig. 1. The schematic of TEC element.

$$\vec{J} = \sigma \vec{E} \tag{9}$$

2.2. Initial conditions and boundary conditions

The initial conditions are as follows. The temperature of the TEC element is uniform and equals to the ambient temperature of $T = 300$ K, and the initial electric potential of the TEC element is 0.

The adopted boundary conditions are: on the top of the heat sink, heat is transferred to the ambient by convective heat transfer, or

$$-\lambda_{\text{sink}} \left.\frac{\partial T}{\partial z}\right|_{z=2(H_0+H_1)+H_2+H_s} = h_{\text{eff}}(T|_{z=2(H_0+H_1)+H_2+H_s} - T_\infty) \tag{10}$$

where h_{eff} is the equivalent convective heat transfer coefficient, which will be determined in the next section.

On the bottom of the TEC element, a constant heat flux is assumed as follows:

$$q_L|_{z=0} = \text{constant} \tag{11}$$

On the side surfaces of the TEC element, the adiabatic boundary conditions are specified, or:

$$\frac{\partial T}{\partial n} = 0 \tag{12}$$

On the internal interfaces between adjacent materials, the temperature and heat flux are assumed to be continuous. The electric boundary conditions for the TEC element are as follows: a fixed current is applied to the TEC element and a zero electric potential is specified on the side surface of connector with $x = 2L_1 + 2L_2$ (Fig. 1) or:

$$I|_{x=0} = \text{constant} \quad 0 < y < L_2, H_0 < z < H_0 + H_1 \tag{13}$$

$$\phi|_{x=2L_1+2L_2} = 0 \quad 0 < y < L_2, H_0 < z < H_0 + H_1 \tag{14}$$

On the other surfaces, the current cannot flow out of the TEC element, thus, we have:

$$\vec{J} \cdot \vec{n} = 0 \tag{15}$$

2.3. Material properties

The n-type and p-type semiconductors are assumed to be $Bi_2(Te_{0.94}Se_{0.06})_3$ and $(Bi_{0.25}Sb_{0.75})Te_3$. Minnich et al. [3] proposed that the properties of some thermoelectric materials are strongly temperature-dependent, hence for the purpose of constructing a general TEC model, the variable properties should be considered. In the present work, the thermal conductivity, electric conductivity and Seebeck coefficient are all assumed to be the functions of temperature as follows:

Table 1
Parameters in Eqs. (16)–(18) for thermoelectric materials ($T_0 = 300$ K).

Material	Thermal conductivity			Electric resistivity			Seebeck coefficient		
	λ_0 (W m^{-1} K^{-1})	A_1 (K^{-1})	A_2 (K^{-2})	ρ_0 (Ω m)	B_1 (K^{-1})	B_2 (K^{-2})	α_0 (V K^{-1})	C_1 (K^{-1})	C_2 (K^{-2})
p-Type	1.472	-1.29×10^{-3}	1.35×10^{-5}	8.826×10^{-6}	5.88×10^{-3}	8.93×10^{-6}	2.207×10^{-4}	1.55×10^{-3}	-3.15×10^{-6}
n-Type	1.643	-9.80×10^{-4}	1.56×10^{-5}	8.239×10^{-6}	4.70×10^{-3}	2.67×10^{-6}	-2.230×10^{-4}	5.62×10^{-4}	-4.65×10^{-6}
Copper	400	0	0	1.700×10^{-9}	0	0	6.500×10^{-6}	0	0

Table 2
Properties for AlN ceramic plate (T = 300 K) [22].

Parameter	Value	Unit
ρ_{cer}	3250	kg m^{-3}
λ_{cer}	260	W K^{-1} m^{-1}
$c_{p,cer}$	7.6×10^5	J kg^{-1} K^{-1}

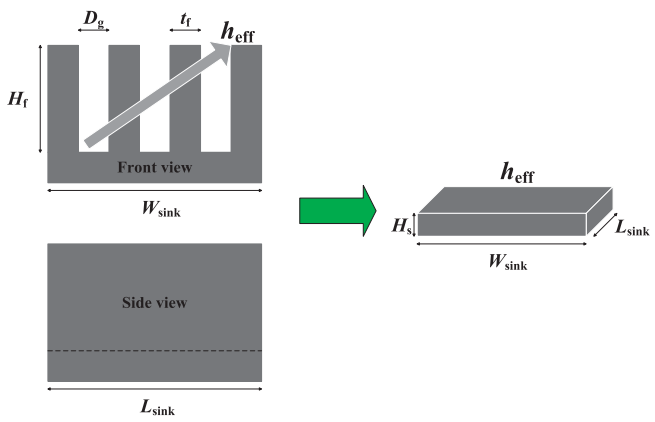

Fig. 2. The schematic of heat sink.

$$\lambda(T) = \lambda(T_0)[1 + A_1(T - T_0) + A_2(T - T_0)^2] \tag{16}$$

$$\frac{1}{\sigma(T)} = \rho(T) = \rho(T_0)[1 + B_1(T - T_0) + B_2(T - T_0)^2] \tag{17}$$

$$\alpha(T) = \alpha(T_0)[1 + C_1(T - T_0) + C_2(T - T_0)^2] \tag{18}$$

where T_0 = 300 K is the reference temperature, $\lambda(T_0)$, $\rho(T_0)$, and $\alpha(T_0)$ are the thermal conductivity, electric resistivity, and Seebeck coefficient at reference temperature, respectively; A_1, A_2, B_1, B_2, C_1, and C_2 are the fitted parameters determined by experimental data as listed in Table 1.

The connector and heat sink are made of copper and their properties are assumed to be constant due to weak thermoelectric effect. AlN is selected as material of ceramic plates and its properties are listed in Table 2 [30].

3. Simplification of heat sink

For a TEC, it is desirable to achieve a high cooling capacity and a large coefficient of performance (COP) through selecting a proper applied current under the same heat sink cooling condition. Thus, for a fair comparison, the heat sink is maintained at the same operation conditions, which means that the equivalent convective heat transfer coefficients h_{eff} in Eq. (10) are the same for all transient simulations.

The most common configuration of heat sink used in current applications is of the fin structure with the geometry shown in Fig. 2. The heat sink comprises a series of parallel fins with height H_f, thickness t_f, and length $L_{sink} = L_2$. Each fin is spaced by a gap D_g and mounted on the heat sink base with an area of $L_{sink} \times W_{sink}$. Air is employed as the coolant. The geometric parameters of the heat sink and the air properties are shown in Table 3 [31,32]. In order to simplify the calculation, the heat sink with real structure is simplified to a flat plate with the same area, which was also adopted by Chen et al. [33]. In order to ensure the same heat dissipation for the equivalent and real heat sinks, the equivalent convective heat transfer coefficient h_{eff} between the equivalent heat sink and the ambient must meet:

Table 3
Properties of heat sink system.

	Parameter	Value	Unit	Source
Fin				
Height	H_f	14.0	mm	[4]
Thickness	t_f	0.2	mm	[4]
Length	L_{sink}	0.5	mm	-
Fin to fin spacing	D_g	0.2	mm	[4]
Base width	W_{sink}	1.4	mm	–
Base height	b_f	0.2	mm	[4]
Coolant (air)				
Thermal conductivity	λ_a	26.3×10^{-3}	W m^{-1} K^{-1}	[23]
Density	ρ_a	1.1614	kg m^{-3}	[23]
Viscosity	μ_a	184.6×10^{-7}	N s m^{-2}	[23]
Specific heat	$c_{p,a}$	1007	J kg^{-1} K^{-1}	[23]

$$Q_H = h_{eff} A (T_{sink}^{top} - T_\infty) \tag{19}$$

where Q_H is the total heat dissipation of real heat sink, T_{sink}^{top} is the top temperature of equivalent plate heat sink, and A is the base area of heat sink, which equals the area of ceramic plate, or $A = L_{sink} \times W_{sink} = L_2 \times (2L_1 \times 2L_2)$.

For a finned structure heat sink, Mereu et al. [31] measured experimentally the relationship between the heat dissipation with heat sink structure and operating conditions, expressed as:

$$Q_H = \frac{\rho_a W_{sink} H_f}{1 + \frac{t_f}{D_g}} \frac{D_g^2}{12\mu_a} \frac{\Delta p}{L_{sink}} c_{p,a} (T_{max} - T_\infty) \tag{20}$$

where ρ_c, μ_c, $c_{p,c}$ are the density, viscosity, and specific heat of air, Δp is the pressure drop across the heat sink, T_{max} is the maximum temperature observed in the heat sink. Copper is adopted as the material of heat sink, and its thermal conductivity is 400 W m^{-1} K^{-1} which is much higher than that of ceramic plate, hence the internal temperature difference of heat sink is expected to be very small. The simulations verify the guess by the fact that the internal temperature difference is less than 0.2 K, therefore, we have $T_{sink}^{top} = T_{max}$. The equivalent heat transfer coefficient can be calculated from Eqs. (19) and (20), or:

$$h_{eff} = \frac{Q_H}{A(T_{max} - T_\infty)} = \frac{\rho_a H_f}{1 + \frac{t_f}{D_g}} \frac{D_g^2}{12\mu_a} \frac{\Delta p}{L_{sink}^2} c_{p,a} \tag{21}$$

In the present work, with Δp = 1.3 Pa, h_{eff} = 7712 W m^{-2} K^{-1}.

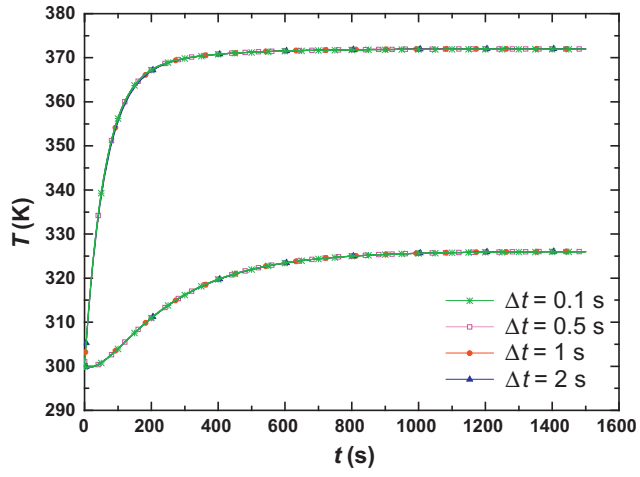

Fig. 3. Independence examination of time step size.

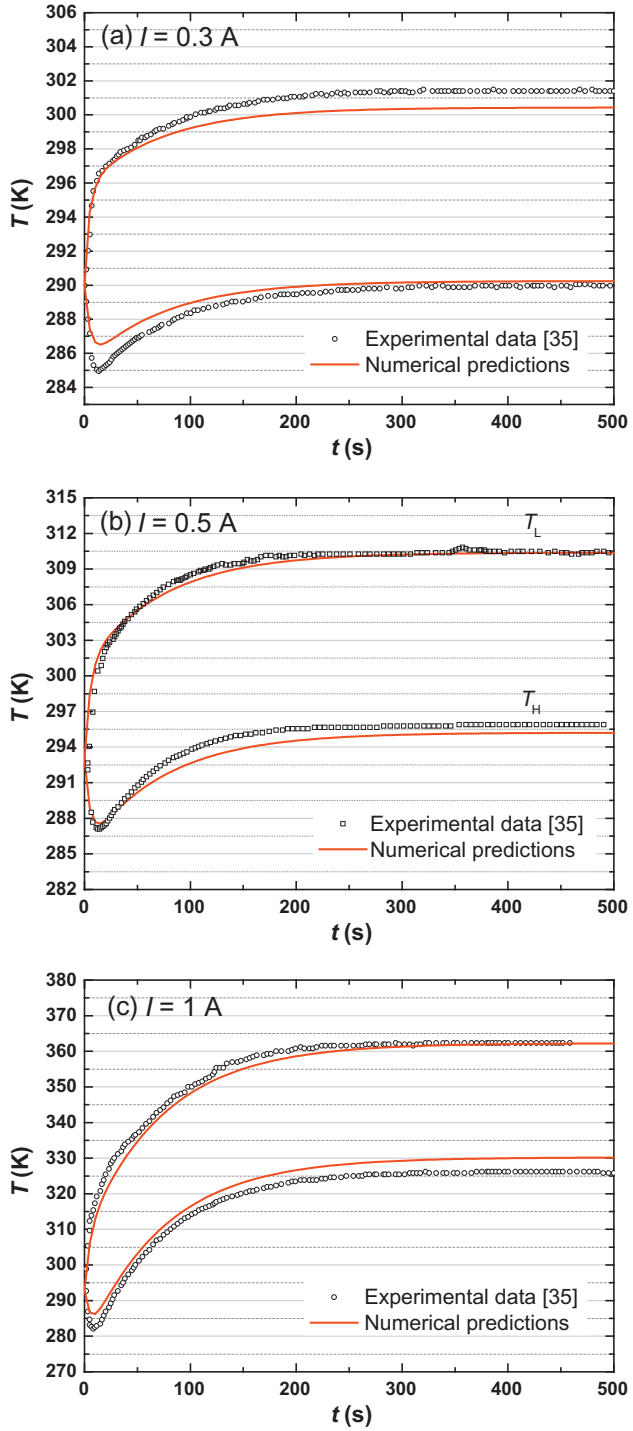

Fig. 4. Comparison of numerical predictions and experimental data: (a) $I = 0.3$ A; (b) $I = 0.5$; (c) $I = 1.0$ A.

4. Model validation

The model used uniformly distributed elements in the x, y and z directions. The grid independence was examined in preliminary test runs. The independence of the time step size was also examined with $\Delta t = 0.1$, 0.5, 1, and 2 s, as shown in Fig. 3, and then $\Delta t = 1$ s was selected.

Cheng et al.'s experimental data [34] are used to validate the present transient model. A zero-cooling-load test is adopted in the present comparison. The reason for performing the zero-cooling-load test is to avoid the errors in measuring the magnitude of the cooling load and the heat losses with it which could lead to uncertainties in the testing conditions [26]. Fig. 4 compares the measurement data regarding the dynamic temperature variations at the cold and hot ends with numerical predictions by the present model at $I = 0.3$, 0.5 and 1 A, respectively. It is found that the predictions agree well with the experiments, the maximum temperature difference between numerical predictions and the measurement data is less than 1.5 K at $I = 0.3$ A, 2.0 K at $I = 0.5$ A, and 4.5 K at $I = 1$ A, respectively, hence, the present transient model can accurately analyze the dynamic characteristics of TECs.

5. Simulation cases

Thermal conductivity, electrical conductivity, and Seebeck coefficient of semiconductor materials are all temperature-dependent. Our previous study [29] has shown that these properties significantly affect the cooling capacity and the COP of TECs when a large temperature gradient occurs within semiconductor materials. For the n-type and p-type semiconductors of $Bi_2(Te_{0.94}Se_{0.06})_3$ and $(Bi_{0.25}Sb_{0.75})Te_3$, with a small applied current, there is no marked difference in the cooling capacity and COP predicted by constant property model and variable property model, however, as the current is larger than 1.2 A, ignoring the property change overestimates the cooling capacity and COP. Especially, note that the constant property model significantly overestimates the maximum working current of TEC, which is defined as the corresponding maximum applied current when the cooling capacity is greater than zero.

In the present work, the TEC geometry and the convective heat transfer coefficient of heat sink remain unchanged, with the same cooling load at the cold end, the response time of temperatures (defined as the consuming time for the temperature of the cold and hot ends reaches the steady-state), the dynamic temperature variations, as well as the steady-state temperatures and temperature difference at the cold and hot ends are closely dependent on the applied current. At different applied currents, the Joule heat and Thomson heat generated within semiconductors have large difference, which leads to a remarkable difference in temperature distributions of semiconductors. Hence, it can be expected that the variable property model could predict the TEC dynamic characteristics more accurately when a large temperature gradient occurs within semiconductors. Therefore, this work focuses on the comparisons of the dynamic characteristics of the TEC predicted by constant and variable property models under different applied currents and different cooling loads at the cold end. The parameters used in the simulations are listed in Table 4, where $I = 0.6$ A, 1.5 A, 2.0 A and 2.8 A denote typical small, medium and large applied currents, respectively, and q_L is varied from 14,285.7 W m^{-2} to 171,428.6 W m^{-2} denoting typical low, medium and high cooling loads at the cold end.

5.1. At small applied current

Fig. 5 shows the dynamic characteristics predicted by the constant and variable property models under different cooling loads at small applied current of $I = 0.6$ A. It can be observed that the response time, the temperature difference between the cold and hot ends, and the temperatures at the cold and hot ends predicted by both models are almost identical. These can be explained by the fact that at small current the Joule heat and the Thomson heat generated inside the semiconductors are very low, leading to a small temperature gradient within the semiconductors, and hence a invisible property change.

Table 4
Cases simulated in the present work.

Cases	I (A)	q_{L1} (W m^{-2})	q_{L2} (W m^{-2})	q_{L3} (W m^{-2})	q_{L4} (W m^{-2})	q_{L5} (W m^{-2})
Low current	0.6	0	14285.7	28571.4	42857.1	71428.6
Medium current	1.5	0	57142.9	85714.3	114285.7	142857.1
	2.0	0	28571.4	71428.6	142857.1	171428.6
Large current	2.8	0	28571.4	71428.6	142857.1	171428.6

Fig. 5 shows that the cold end temperature decreases but the hot end temperature increases with the time increased. However, both gradually approach to the steady-state. With the increase in the cooling load, the temperatures at the cold and hot ends are both increased, but the temperature rising rate of the cold end is much higher than that of the hot end, resulting in a significant reduction in the temperature difference between the cold and hot ends. This is responsible for that with the same h_{eff} and I, only a low temperature difference can reduce Fourier's thermal conduction, hence the TEC maintains a high cooling capacity. It is noted that, since the temperature difference decreases and the steady-state temperature at the cold end is closer to the initial temperature of 300 K under high cooling load, the TEC response time is significantly reduced as the cooling load increases.

5.2. At medium applied current

Fig. 6 shows the dynamic temperature variations at the cold and hot ends predicted by the constant and variable property models at I = 1.5 A with various cooling loads. With zero cooling load, the dynamic temperature variations at the cold end are almost the same with that at the hot end, only a slightly difference occurs when t > 200 s. The two models both predict the temperature overshoot phenomenon at the hot end, for example, the variable property model indicates that the hot end temperature increases rapidly from the initial stage of 300 K, then decreases slowly after reaching the maximum value of 348.1 K, finally approaches to the steady value of 342 K at the time of 1200 s.

The constant and variable property models predict that, at I = 1.5 A the temperatures at the cold and hot ends both increase with the increase in the cooling load, which has been observed at small current of 0.6 A (Fig. 5). However, at medium current of 1.5 A, the difference in dynamic temperature variation predicted by both models occurs and the difference become more remarkable at high cooling load. The constant property model underestimates the temperatures at the cold and hot ends. In details, the steady-state temperatures at the hot end and cold end predicted by the constant property model under q_L = 85,714.3 W m^{-2} is 347.8 K, and 281.6 K, which underestimates by 6.8 K and 6.7 K compared to the variable property model, respectively. Under q_L = 142,857.1 W m^{-2}, however, the underestimations increase to 11.0 K and 14.7 K at the hot end and cold end, respectively. Fig. 7 shows the temperature distributions within p- and n-type semiconductors predicted by both models under q_L = 142,857.1 W m^{-2}, and t = 1000 s. It can be seen that the temperature predicted by the constant property model is lower than that by the variable property model. According to Eqs. (2) and (3), the reason can be explained. Because the electrical conductivities of $Bi_2(Te_{0.94}Se_{0.06})_3$ and $(Bi_{0.25}Sb_{0.75})Te_3$ have negative temperature effect, the constant property model underestimates the Joule heat generated within the semiconductors, leading to a lower temperature distribution (Fig. 7).

Note that with high cooling loads of q_L = 114,285.7 W m^{-2} and 142,857.1 W m^{-2}, a undershoot phenomenon of cold end temperature is observed (Fig. 7c and d). The cold end temperature decreases from 300 K to the minimum value at the initial stage, then increases until reaching the steady-state. This phenomenon can be explained as follows: the Peltier cooling occurs at the cold end of the semiconductors, while the Joule heating and Thomson effect occurs uniformly across the semiconductors columns. During the dynamic process, the cooling at the cold end occurs before the Joule heat and Thomson heat reach this end and a temporary temperature overshoot at the cold end can be observed. However, for small q_L, there is a large temperature differences between the cold and hot ends, leading to a enhanced Fourier's back heat conduction from the hot end to the cold end, hence the undershoot does not occur.

Fig. 8 shows the electric potential difference and COP (= $Q_L/P = Q_L/IV$, where $Q_L = q_L A$ is the cooling capacity of the TEC, P is the electric power, V is the electric potential difference) predicted by the constant and variable property models at I = 1.5 A. It can be seen that due to the negative temperature effect of electric conductivity for $Bi_2(Te_{0.94}Se_{0.06})_3$ and $(Bi_{0.25}Sb_{0.75})Te_3$ materials, the variable property model predicts higher electric potential difference through the TEC. Therefore, more electric power is needed for the variable property model, leading to a reduced COP.

Fig. 9 shows the dynamic temperature variations at the cold and hot ends at I = 2.0 A with q_L = 0 W m^{-2} and 142,857.1 W m^{-2}. It is noted that at the larger applied current of I = 2.0 A, there is a remarkable difference between the constant and variable models even at zero cooling load due to significantly enhanced Joule heat. With high cooling load q_L = 142857.1 W m^{-2}, the temperature at the cold end predicted by the variable property model does not decreases but increases continuously to steady-state value of 392.4 K, which is even higher than the temperature at the hot end predicted by constant property model. The results again confirm that temperature-dependent properties have significant effect on dynamic characteristics of the TEC.

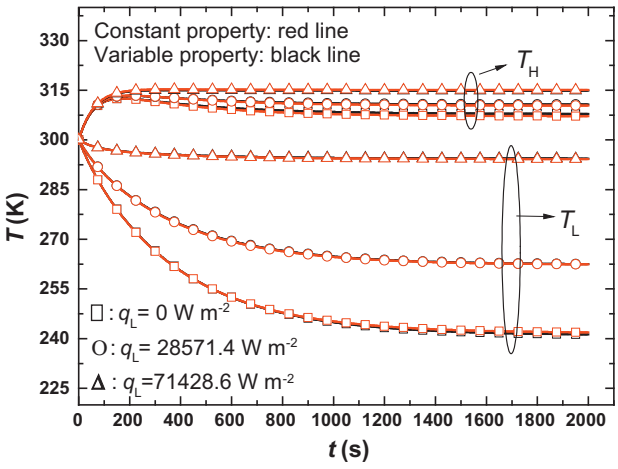

Fig. 5. Dynamic temperature variations at the cold and hot ends predicted by constant and variable property models at I = 0.6 A.

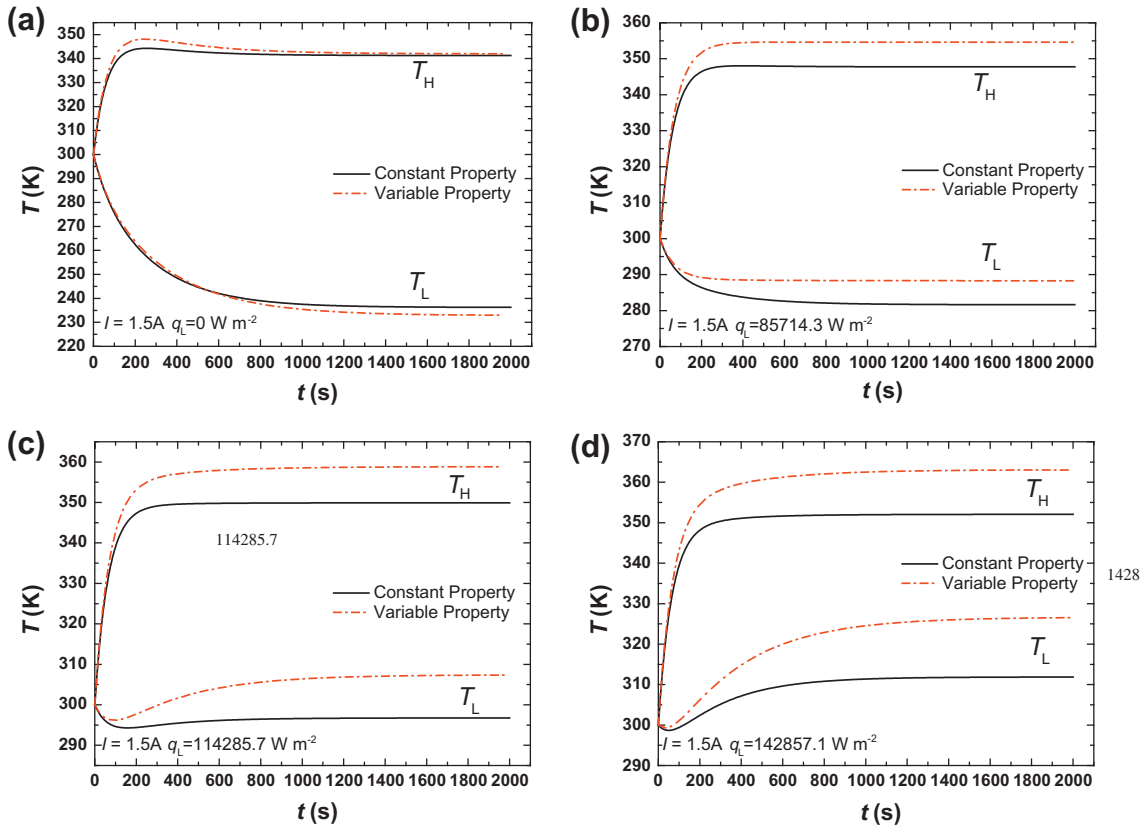

Fig. 6. Dynamic temperature variations at the cold and hot ends predicted by constant and variable property models at $I = 1.5$ A: (a) $q_L = 0$ W m^{-2}, (b) $q_L = 85{,}714.3$ W m^{-2}, (c) $q_L = 114{,}285.7$ W m^{-2}, (d) $q_L = 142{,}857.1$ W m^{-2}.

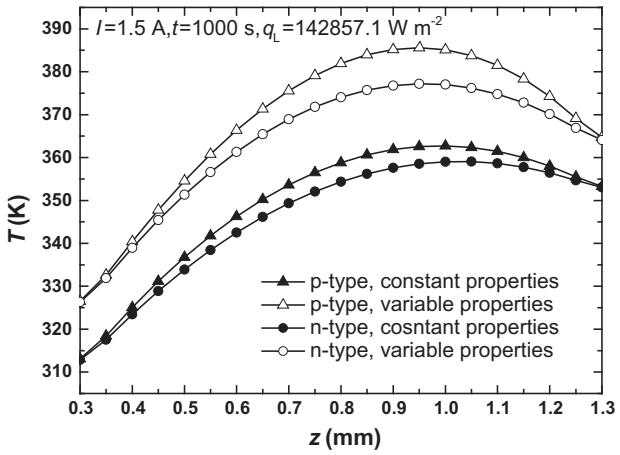

Fig. 7. Temperature distributions within semiconductors predicted by constant and variable property models at $I = 1.5$ A.

5.3. At large applied current

Fig. 10 shows the dynamic temperature variations at the cold and hot ends at $I = 2.8$ A with $q_L = 0$ W m^{-2} and 142,857.1 W m^{-2}, respectively. At large applied current, the temperature gradient within the semiconductors is significantly elevated due to the strong Joule heating, resulting in strong effect of material properties. Consequently, dynamic temperature variations at the cold and hot ends predicted by constant property model remarkably differ from those predicted by variable property model. The constant property model predicts $T_L = 295.0$ K and $T_H = 430.2$ K at $q_L = 0$ W m^{-2}, while $T_L = 348.3$ K and $T_H = 438.8$ K at $q_L = 142{,}857.1$ W m^{-2} when the TEC element approaches the steady-state. However, the variable property model indicates that the temperatures at the cold and hot ends increase rapidly, and it can never reach the steady-state

Using our previous steady-state model [29], the I–Q_L performance curves with fixed temperatures at the cold and hot ends, $T_L = 295.0$ K and $T_H = 430.2$ K, as well as $T_L = 348.3$ K and $T_H = 438.8$ K, can be predicted as shown in Fig. 11. The black lines are predicted by constant property model, and red dash dot lines are predicted by variable property model. Note that the hollow circle in I–Q_L curve (constant property model, $T_L = 295.0$ K and

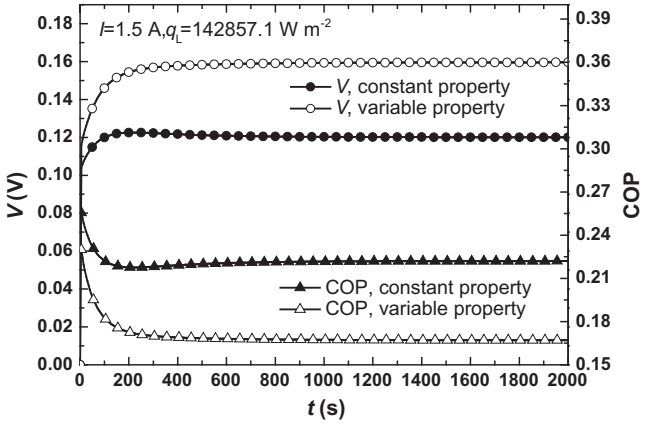

Fig. 8. The electric potential difference and COP predicted by constant and variable property models at $I = 1.5$ A.

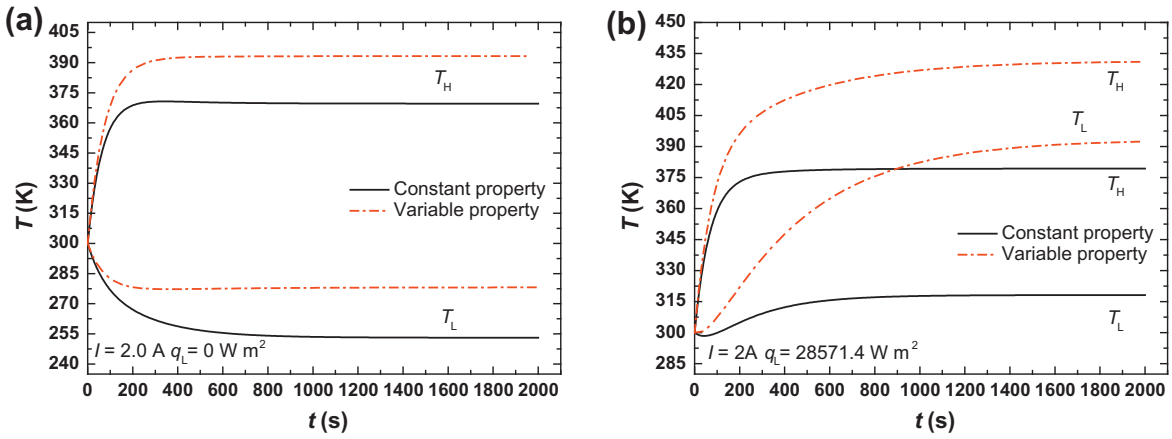

Fig. 9. Dynamic temperature variations at the cold and hot ends predicted by constant and variable property models at $I = 2.0$ A: (a) $q_L = 0$ W m^{-2}, (b) $q_L = 142{,}857.1$ W m^{-2}.

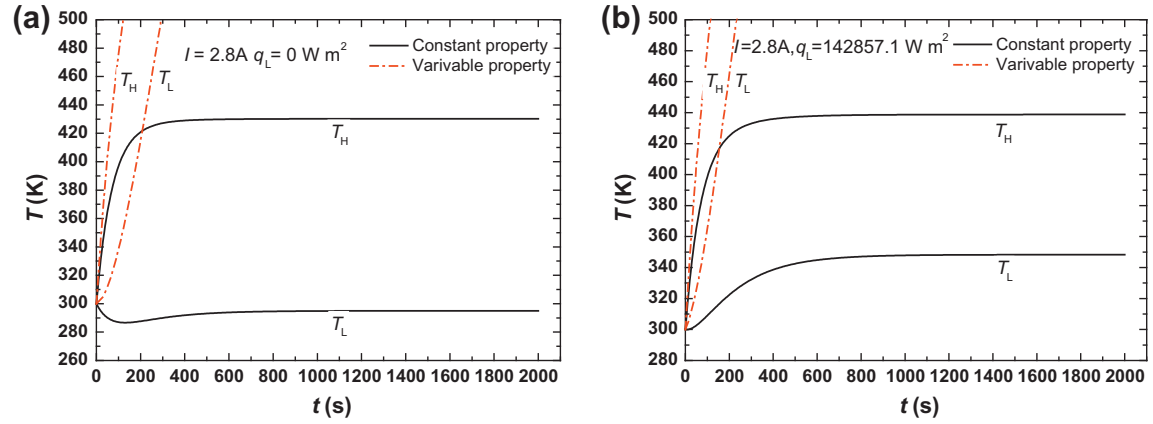

Fig. 10. Dynamic temperature variations at the cold and hot ends predicted by constant and variable property models at $I = 2.8$ A: (a) $q_L = 0$ W m^{-2}, (b) $q_L = 142{,}857.1$ W m^{-2}.

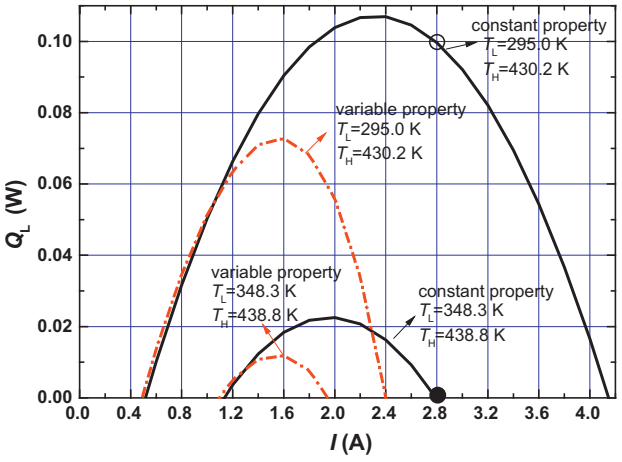

Fig. 11. Cooling capacity of TEC at different temperature difference between the cold and hot ends predicted by constant and variable property models.

$T_H = 430.2$ K) denotes the steady-state point with $I = 2.8$ A and $Q_L = 0.1$ W ($q_L = Q_L/A = 142{,}857.1$ W m^{-2}), the solid circle in I–Q_L curve (constant property model, $T_L = 348.3$ K and $T_H = 438.8$ K) denotes the steady-state point with $I = 2.8$ A, $Q_L = 0$ W. The result indicates that the transient model developed in this work can predict well the dynamic response characteristics and the final steady-state. The variable property model predicts that the effective working current ranges from 0.49 A to 2.40 for fixed $T_L = 295.0$ K and $T_H = 430.2$ K, and from 1.09 A to 1.94 A for fixed $T_L = 295$ K and $T_H = 430.2$ K. Apparently, for the transient cases, applied current $I = 2.8$ A is higher than the maximum working current. Under this circumstance, the heat transferred from the hot end to the cold end by Fourier's heat conduction is still larger than the heat adsorbed at the cold end by Peltier effect even at zero cooling load, thus, the temperatures at the cold and hot ends both increase resulting the failure of TEC refrigeration.

6. Conclusions

This work develops a complete three-dimensional transient TEC model, which introduces the coupling of the heat transfer and electric conduction within semiconductors, and the transient TEC model developed in this paper has not been found in the existing literatures. The developed model is used to investigate the dynamic characteristics of TECs. A miniature TEC element with a finned structure heat sink is investigated and $Bi_2(Te_{0.94}Se_{0.06})_3$ and $(Bi_{0.25}Sb_{0.75})Te_3$ are selected as the n-type and p-type thermoelectric materials, respectively. The present model predicts that dynamic temperature variations at cold and hot ends under zero cooling load agree well with experimental results.

Three types of operating conditions including small, medium, and large applied currents are adopted to examine the effect of material properties on the dynamic characteristics of the TEC. The results show that at small currents the constant and variable

property models predict almost the same dynamic characteristics; at medium currents the predictions of two models differ, and the difference is more apparent at high cooling load; at large currents the variable property model predict that the temperatures at cold and hot ends increase continuously and never reach the steady-state, oppositely, the constant property model predict that the TEC still supply refrigeration. The present simulations indicate that the variable property model is more appropriate to accurate predict TEC transient performance, especially when the TEC operates at medium and high applied currents.

At a specific applied current, the temperatures at the cold and hot ends both increase with the elevated cooling load, but the temperature rising rate of the cold end is much higher than that of the hot end, resulting in a significant reduction in the temperature difference between the cold and hot ends. This phenomenon can be attributed to that small temperature difference reduces Fourier's back heat transfer and hence maintains the high cooling capacity of TECs. The response time of the TEC varies from several hundreds of seconds to several thousands of seconds, which is dependent on its operating conditions.

Acknowledgement

This study was supported by the National Natural Science Foundation of China (No. 51276060), by National Basic Research Program of China (No. 2009CB219803), by Program for New Century Excellent Talents in University (No. NCET-11-0635), and by the Fundamental Research Funds for the Central Universities (No. 11ZG01).

References

[1] Riffat SB, Ma X. Thermoelectrics: a review of present and potential applications. Appl Therm Eng 2003;23:913–35.
[2] Rowe DM, editor. Thermoelectrics handbook: macro to nano. Boca Raton: CRC Press; 2006.
[3] Minnich AJ, Dresselhaus MS, Ren ZF, Chen G. Bulk nanostructured thermoelectric materials: current research and future prospects. Energy Environ Sci 2009;2:466–79.
[4] Huang BJ, Duang CL. System dynamic model and temperature control of a thermoelectric cooler. Int J Refriger 2000;23:197–207.
[5] Völklein F, Min G, Rove DM. Modeling of microelectromechanical thermoelectric cooler. Sensors Actuators 1999;75:95–101.
[6] Huang BJ, Chin CJ, Duang CL. A design method of thermoelectric cooler. Int J Refriger 2000;23:208–18.
[7] Xuan XC, Ng KC, Yap C, Chua HT. A general model for studying effects of interface layers on thermoelectric devices performance. Int J Heat Mass Transfer 2002;45:5159–70.
[8] Huang MJ, Yen RH, Wang AB. The influence of the Thomson effect on the performance of a thermoelectric cooler. Int J Heat Mass Transfer 2005;48:413–8.
[9] Cheng YH, Shih C. Maximizing the cooling capacity and COP of two-stage thermoelectric coolers through genetic algorithm. Appl Therm Eng 2006;26:937–47.
[10] Pan Y, Lin B, Chen J. Performance analysis and parametric optimal design of an irreversible multi-couple thermoelectric refrigerator under various operating conditions. Appl Energy 2007;84:882–92.
[11] Lee KH, Kim OJ. Analysis on the cooling performance of the thermoelectric micro-cooler. Int J Heat Mass Transfer 2007;50:1982–92.
[12] Yu J, Wang B. Enhancing the maximum coefficient of performance of thermoelectric cooling modules suing internally cascaded thermoelectric couples. Int J Refriger 2009;32:32–9.
[13] Chen WH, Liao CY, Huang CI. A numerical study on the performance of miniature thermoelectric cooler affected by Thomson effect. Appl Energy 2012;89:464–73.
[14] Small-scale energy harvesting. In: Lallart M. Three dimensional TCAD simulation of a thermoelectric module suitable for use in a thermoelectric energy harvesting system, Could C, Shammas N, InTech; 2012. [Chapter 2]
[15] Gou XL, Xiao H, Yang SW. Modeling, experimental study and optimization on low-temperature waste heat thermoelectric generator system. Appl Energy 2010;87:3131–6.
[16] Kim SH. Analysis and modeling of effective temperature differences and electrical parameters of thermoelectric generators. Appl Energy 2013;102:1458–63.
[17] Suter C, Jovanovic ZR, Steinfeld A. A 1 kW_e thermoelectric stack for geothermal power generation – modeling and geometrical optimization. Appl Energy 2012;99:379–85.
[18] van Sark WGJHM. Feasibility of photovoltaic – thermoelectric hybrid modules. Appl Energy 2011;88:2785–90.
[19] Qiu K, Hayden ACS. Integrated thermoelectric and organic Rankine cycles for micro-CHP systems. Appl Energy 2012;97:667–72.
[20] Patyk A. Thermoelectric generators for efficiency improvement of power generation by motor generators – environmental and economic perspectives. Appl Energy 2013;102:1448–57.
[21] He W, Su YH, Riffat SB, Hou JX, Ji J. Parametrical analysis of the design and performance of a solar heat pipe thermoelectric generator unit. Appl Energy 2011;88:5083–9.
[22] Hsu CT, Huang GY, Chu HS, Yu B, Yao DJ. Experiments and simulations on low-temperature waste heat harvesting system by thermoelectric power generators. Appl Energy 2011;88:1291–7.
[23] Alata M, Al-Nimr MA, Naji M. Transient behavior of a thermoelectric device under the hyperbolic heat conduction model. Int J Thermophys 2003;26:1753–68.
[24] Montecucco A, Buckle JR, Knox AR. Solution to the 1-D unsteady heat conduction equation with internal Joule heat generation for thermoelectric devices. Appl Therm Eng 2012;35:177–84.
[25] Taylor PJ, Jesser WA, Rosi FD, Derzko Z. A model for the non-steady-state temperature behaviour of thermoelectric cooling semiconductor devices. Semiconductor Sci Technol 1997;12:443–7.
[26] Cheng CH, Huang SY, Cheng TC. A three-dimensional theoretical model for predicting transient thermal behavior of thermoelectric coolers. Int J Heat Mass Transfer 2010;53:2001–11.
[27] Thonhauser T, Mahan GD, Zikatanov L, Roe J. Improved supercooling in transient thermoelectrics. Appl Phys Lett 2004;85:3247–9.
[28] Yang RG, Chen G, Ravi Kumar A, JeffreySnyder G, Jean-Pierre Fleurial. Transient cooling of thermoelectric coolers and its applications for microdevices. Energy Conv Manage 2005;46:1407–21.
[29] Wang XD, Huang YX, Cheng CH, Lin DTW. A three-dimensional numerical modeling of thermoelectric device with consideration of coupling of temperature field and electric potential field. Energy 2012;47:488–97.
[30] Qin ML, Qu XH, Lin JL, Xiao PA, Zhu BJ, Tang CF. Progress in research and development of aluminum nitride (AlN) ceramics. Rare Metal Mater Eng 2002;31:8–12.
[31] Mereu S, Sciubba E, Bejan A. The optimal cooling of a stack of heat generating boards with fixed pressure drop, flowrate or pumping power. Int J Heat Mass Transfer 1993;36:3677–86.
[32] Incropera FR, Dewitt DP, Bergman TL, Lavine AS. Fundamentals of heat and mass transfer. 6th ed. Hoboken: John Wiley & Sons; 2007.
[33] Wang CC, Hung CI, Chen WH. Design of heat sink for improving the performance of thermoelectric generator using two-stage optimization. Energy 2012;39:236–45.
[34] Chen CH, Huang SY. Development of a non-uniform-current model for predicting transient thermal behavior of thermoelectric coolers. Appl Energy 2012;100:326–35.